Journal of Medicinal Chemistry

Article

pubs.acs.org/jmc

X-ray Absorption Spectroscopy of an Investigational Anticancer Gallium(III) Drug: Interaction with Serum Proteins, Elemental Distribution Pattern, and Coordination of the Compound in Tissue

Alfred A. Hummer,[†] Caroline Bartel,[‡] Vladimir B. Arion,[‡] Michael A. Jakupec,[‡] Wolfram Meyer-Klaucke,[§] Tina Geraki,[∥] Paul D. Quinn,[∥] Ana Mijovilovich,[⊥] Bernhard K. Keppler,[‡] and Annette Rompel*[,†]

[†]Institut für Biophysikalische Chemie, Universität Wien, Althanstraße 14, 1090 Wien, Austria

[‡]Institut für Anorganische Chemie, Universität Wien, Währinger Straße 42, 1090 Wien, Austria

[§]European Molecular Biology Laboratory Hamburg, Notkestraße 85, 22603 Hamburg, Germany

[∥]Diamond Light Source, Harwell Campus, Didcot OX11 0DE, United Kingdom

[⊥]Inorganic Chemistry and Catalysis Group, Debye Institute for Nanomaterials Science, Utrecht University, Universiteitsweg 99, 3584 CG Utrecht, The Netherlands

ABSTRACT: Tris(8-quinolinolato)gallium(III) (**1**, KP46) is a very promising investigational anticancer drug. Its interaction with serum proteins, elemental distribution, and coordination in tissue were investigated with X-ray absorption (XAS) methods. Model compounds with mixed O, N, and/or S donor atoms are reported. The coordination and structure of **1** in cell culture medium (minimum essential medium, MEM) and fetal calf serum (FCS) were probed by XANES and EXAFS. The interaction of **1** with the serum proteins apotransferrin (apoTf) and human serum albumin (HSA) was addressed as well. By application of micro-XAS to tissue samples from mice treated with **1**, the gallium distribution pattern was analyzed and compared to those of physiological trace elements. The complex **1** turned out to be very stable under physiological conditions, in cell culture media and in tissue samples. The coordination environment of the metal center remains intact in the presence of apoTf and HSA. The gallium distribution pattern in tumor and liver tissue revealed high similarities to the distribution patterns of Zn and Fe, minor similarities to Cu and Ni, and no similarity to Ca.

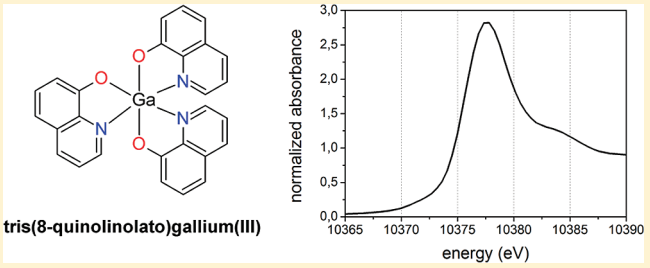

INTRODUCTION

Tris(8-quinolinolato)gallium(III) (**1**, KP46)[1,2] (Figure 1) is a metal complex currently studied as an anticancer drug, which shows promise to be superior to simple gallium salts in terms of antitumor activity.[2−4] The anticancer properties of gallium were discovered in 1971,[5,6] and in the mid-1970s gallium nitrate had entered first clinical trials.[7] The main drawbacks of a therapy with gallium nitrate and other gallium salts were the need for slow, long-term infusion to avoid toxicities associated with high plasma levels of gallium, the poor bioavailability when given via the oral route, and the loss of tumor selectivity when present in higher concentrations in plasma.[8] These issues could be circumvented by the application of novel gallium complexes like tris(3-hydroxy-2-methyl-4*H*-pyran-4-onato)gallium(III) (gallium maltolate) and **1**.[1,9,10] With these complexes higher tissue and serum concentrations with a smaller number of applications could be achieved.[11] Furthermore, **1** circumvented unicellular and multicellular resistances[12] and showed antiproliferative activity in cell lines expressing multidrug resistance-associated protein (MRP) and lung resistance protein (LRP).[8] In a phase I clinical trial seven patients were treated with **1**; out of those, four had renal cell carcinoma and three had other carcinomas (head and neck, stomach, ovaries).[3] Most remarkably, orally administered **1** yielded long-lasting disease stabilization in two patients and one partial remission of renal cell carcinoma.[3,13] Furthermore, preclinical studies suggest its suitability for the treatment of malignant melanoma.[14]

The uptake pathway and mode of action are relatively well understood for gallium nitrate and gallium chloride[8,15] but remain elusive for the gallium complexes. The uptake of gallium nitrate through the transferrin receptor into the cell and the subsequent inhibition of ribonucleotide reductase are considered as the critical steps in the mechanism of action.[16,17] Gallium is bound to the iron dependent M2 subunit of ribonucleotide reductase and causes a halt in the production of deoxynucleoside triphosphates (dNTPs), which in turn stops DNA synthesis and arrests the cell cycle in the S-phase.[8] **1** on the other hand is a relatively stable coordination compound, and therefore, different uptake pathways are conceivable.[15] High concentrations of iron in the cell culture medium induced resistance to gallium salts.[18] The resistant and sensitive cells showed the same rate of Ga uptake, but the resistant cells were able to increase the iron level significantly and overcome inhibition through Ga in this way.

Received: April 17, 2012
Published: May 24, 2012

   dx.doi.org/10.1021/jm3005459 | *J. Med. Chem.* 2012, 55, 5601−5613

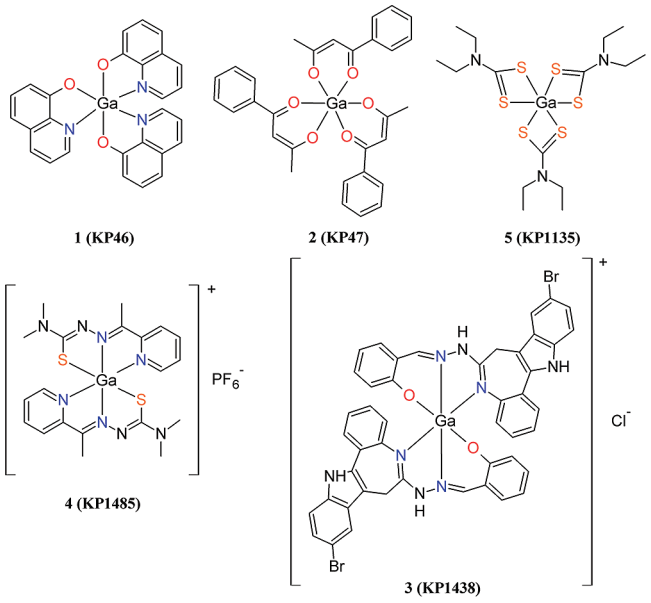

Figure 1. Gallium model compounds.

The resistance to Ga salts was ascribed to an up-regulation of the transferrin receptor.[18] Considerable differences in the mode of action of **1** in comparison to gallium salts or more soluble complexes are likely.

X-ray absorption spectroscopy (XAS)[19] allows for the investigation of the oxidation state, the coordination environment of a metal site, and the elemental distribution of metals in biological systems. This method has two main advantages. First, it needs no long-range order, and second, it offers the possibility to investigate spectroscopically silent elements.[20] Hence, metals like Au(I), Zn(II), and Ga(III) possessing a full or empty d-shell are ideal candidates for the investigation by XAS. Especially gallium is well suited for investigation by this method, as it does not occur naturally in biological tissues. This fact makes it possible to study the overall average oxidation state and coordination environment by bulk XAS techniques. Micro-XAS mapping, using a highly focused X-ray beam, gives us the opportunity to study the gallium distribution pattern in different tissues and regions thereof. At selected spots in the tissue micro-XANES gives information about the local coordination environment. The low concentration of **1** in mouse tissue was one of the major obstacles encountered in biological experiments, in particular in the micro-XAS regime. Using a third generation X-ray light source in combination with an ultra low temperature sample space and a highly sensitive multielement solid state detector enabled the study of this compound in biological tissue. While the high photon flux (about 4×10^{12} ph/s) of a third generation synchrotron is an advantage in terms of very dilute samples, it also incorporates the danger of photoreduction of the metal site under study and increased overall sample degradation.[21−23] To overcome or minimize sample degradation, low temperature sample environments are used. The lower photon flux of a second generation facility causes lesser X-ray damage but lowers the signal-to-noise ratio.[21] In this study spectra were collected on both types of synchrotrons, the second generation DESY and the third generation DLS, allowing us to directly compare data taken at different generations of synchrotrons and to reveal the real situation in a biological environment.

In this study we report the X-ray absorption near edge spectroscopy (XANES) and extended X-ray absorption fine structure (EXAFS) spectra of gallium model compounds with known coordination spheres. XANES was used to investigate the oxidation state and coordination motif, whereas EXAFS was used to determine the type, amount, and distance of the first shell atoms. The coordination environment of **1** in the presence of different serum proteins and in tissue samples from mice treated with **1** was investigated with XAS. Micro-XAS mapping of the tissue samples was performed to resolve the elemental distribution. At gallium hot spots on the tissue XANES spectra were recorded. Acquiring information about the possible interaction of **1** with serum proteins and the determination of the coordination environment of gallium(III) in mouse tissue are the main targets in this study.

RESULTS

XANES. *Model Compounds.* XANES spectroscopy has been applied to the ionic compound $Ga(NO_3)_3$, the tetrahedral $[GaCl_4]^-$ complex anion, and five octahedral complexes with mixed S/N/O first shell environments. The following model compounds were investigated by XAS measurements: **1** (with first coordination sphere GaO_3N_3),[1,2] tris(1-phenyl-1,3-butanedionato-*O*,*O*′)gallium(III) (**2**, KP47, GaO_6),[24] bis{*N*-(9-bromo-7,12-dihydroindolo[3,2-*d*][1]benzazepin-6-ylidene)-*N*′-(2-oxidobenzylidene)hydrazone-*N*,*N*′,*O*}gallium(III) chloride (**3**, KP1438, GaO_2N_4),[25] bis(2-acetylpyridine *N*,*N*′-dimethylthiosemicarbazonato)-*N*,*N*,*S*-gallium(III) hexafluorophosphate (**4**, KP1485, GaS_2N_4),[26] tris(*N*,*N*-diethyldithiocarbamato-*S*,*S*′)-gallium(III) (**5**, KP1135, GaS_6),[27,28] tetraethylammonium tetrachlorogallate (**6**, $[GaCl_4]^-$), and gallium nitrate decahydrate (**7**, $Ga(NO_3)_3 \cdot 10H_2O$).[29−31] Structural formulas are shown in Figure 1.

The XANES spectra of the model compounds and their first derivatives are shown in Figure 2. With increasing electronegativity of the surrounding atoms the edge positions are shifted to higher energies. The edge position of **1** was determined to be 10 375.5 eV by the maximum in the first derivative. The spectrum shows no pre-edge feature and has a sharply rising white line and an additional feature at about 10 385 eV past the edge. The peak at 10 385 eV is also seen in the reference compound β-Ga_2O_3, where it was ascribed to multiple scattering events occurring during the absorption process.[32] In comparison to **1** (GaO_3N_3), the tetrahedral **6** anion has the lowest energy position (−2.8 eV), whereas **2** (GaO_6) exhibits the highest energy position shifted by +0.5 eV (see Table 1). The edge positions of **3** (GaO_2N_4) and **1** (GaO_3N_3) are the same, reflected by their nearly identical coordination environment (O_2N_4 and O_3N_3).

The white line peaks are all about 2.5 AU except for **6**. For **6** the number of first shell scatterers is reduced to four chlorine atoms with a tetrahedral configuration. The finding of a lowered energy position is in agreement with a study of Nishi et al.[32] where gallium oxides containing different coordination environments were investigated (tetrahedral Ga(t) and octahedral Ga(o)). The edge position of **6** was determined to be 10 372.7 eV, which is even 1 eV below the one for Ga(t) (10 373.6 eV). In addition the spectra of Ga(t) and **6** are very similar in shape.

The sulfur containing model compounds have the edge at lower energy: 10 373.6 eV for **5** (GaS_6) and 10 374.1 eV for **4** (GaS_2N_4). There are no significant additional features in the spectra except postedge shoulders at about 10 377 eV for **5** (GaS_6) and 10 382 eV for **4** (GaS_2N_4). The edge position of the ionic **7** occurs at 10 375.0 eV.

KP46 in Presence of MEM, FCS, apoTf, and HSA. In comparison to well-known metal based drug candidates such as

dx.doi.org/10.1021/jm3005459 | J. Med. Chem. 2012, 55, 5601−5613

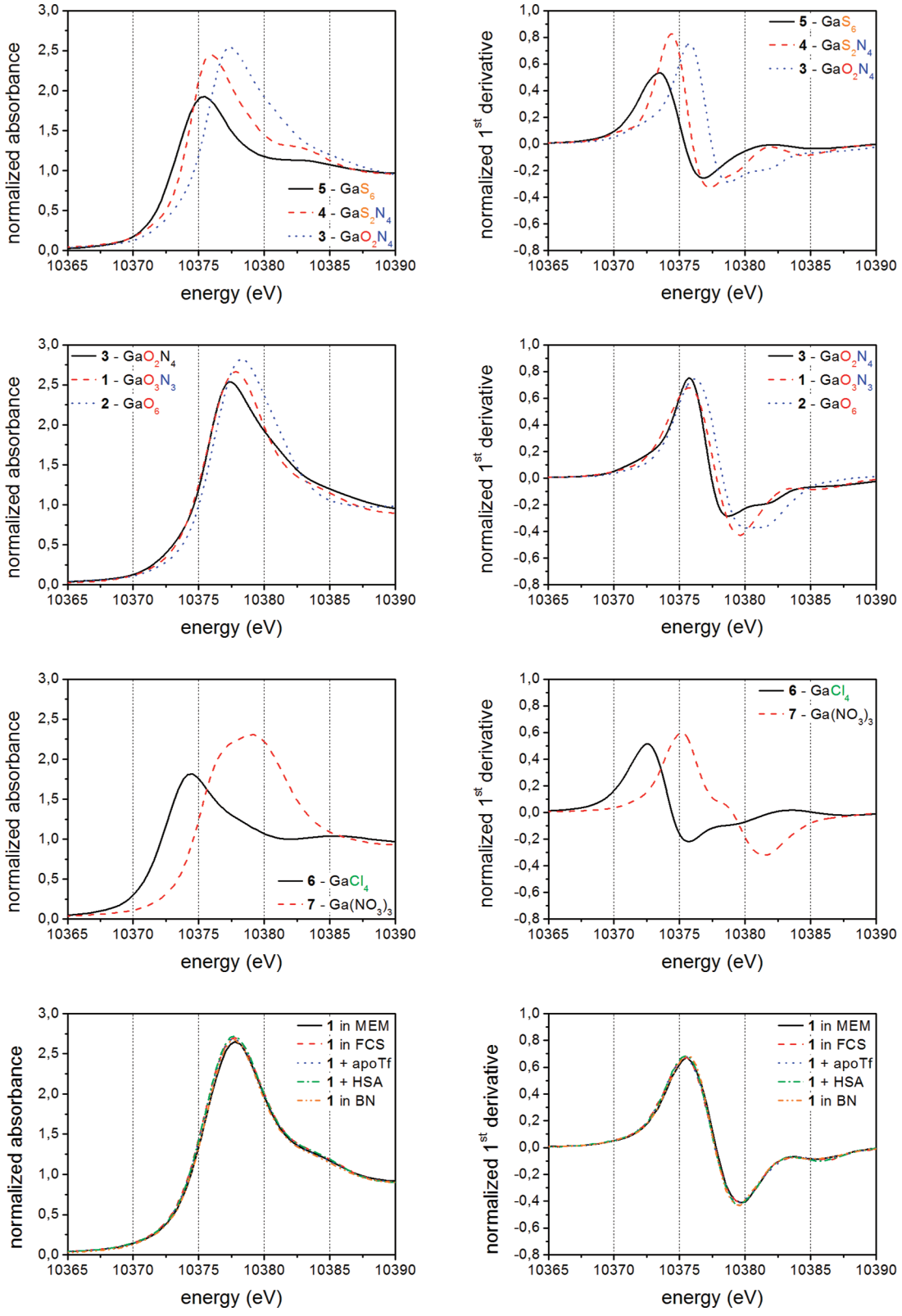

Figure 2. Normalized spectra and first derivatives of the model compounds and of **1** in the presence of minimum essential medium, fetal calf serum, apotransferrin, and human serum albumin and as BN preparation.

2-acetylpyridine-4,4-dimethyl-3-thiosemicarbazonato-*N*,*N*,*S*-dichloridogallium(III) (KP1492, log P = −1.40)[26] and 2-acetylpyridine-*N*-pyrrolidinyl-3-thiosemicarbazonato-*N*,*N*,*S*-dichloridogallium(III) (KP1497, log P = −0.69),[26] **1** is a lipophilic compound with its log P of 0.88.[8,33] Therefore, the mode of action of **1** is supposed to be different from those of the gallium salts.[8] Fetal calf serum (FCS) and minimum essential medium (MEM) are widely used in cell culture. FCS and MEM were used to model the chemical environment during the application in vitro. The main components of MEM are amino

dx.doi.org/10.1021/jm3005459 | J. Med. Chem. 2012, 55, 5601−5613

Table 1. Model Compounds and Edge Shifts

compd	first coord shell	coord or concn [mM]	edge energy [eV]	shift to **1** [eV]
6	$GaCl_4$	tetrahedral	10372.7	−2.8
5	GaS_6	octahedral	10373.6	−1.9
4	GaS_2N_4	octahedral	10374.1	−1.4
3	GaO_2N_4	octahedral	10375.5	+0.0
1	GaO_3N_3	octahedral	10375.5	+0.0
2	GaO_6	octahedral	10375.9	+0.5
7	GaO_6	ionic compd	10375.0	−0.5
1 in MEM		1 mM	10375.5	
1 in FCS		1 mM	10375.4	
1 + HSA		1:1 mM	10375.4	
1 + apoTf		1:1 mM	10375.4	
tumor DLS			10375.4	
tumor DESY			10375.5	
liver DLS			10375.3	
liver DESY			10375.5	

acids, salts (Ca, K, Mg, Na), and glucose, while FCS mainly consists of bovine albumin and growth factors like α-, β-, and γ-globulines with a low concentration in antibodies.[34,35]

Two transport proteins were envisaged as binding partners of **1** potentially involved in the transport via the bloodstream to the target site: apo-transferrin (apoTf) and human serum albumin (HSA). These two are the most relevant transport proteins for transition metals in vivo.[36]

XANES spectra have been collected for **1** in MEM, in FCS, and in the presence of apoTf and HSA. The normalized XANES spectra of these four samples and their first derivatives are shown in Figure 2. Again, the edge position was determined over the maximum in the first derivative. The edge positions of **1** in MEM and FCS and of **1** in the presence of apoTf and HSA are reported in Table 1. For all four solution spectra the edge energies vary only between 10 375.4 and 10 375.5 eV, which indicates no edge shifts. The heights of the white lines are about 2.7 AU. All spectra show a postedge peak at around 10 385 eV, typical for **1**. Moreover the XANES patterns of all liquid samples resembled that of solid **1**. The absence of any significant changes in the spectra of **1** in solution implies an intact octahedral coordination geometry throughout the different samples. **1** is a relatively stable complex, with gallium forming strong bonds to its ligands via oxygen and nitrogen atoms, and no ligand dissociation could be observed under these mild conditions. Therefore, a direct binding to the Ga metal site is ruled out. As XAS measures the average signals from all Ga atoms, this is valid for the bulk of the Ga atoms present in the sample.

EXAFS. *Model Compounds.* The extracted fine structures and the Fourier transforms are shown in Figure 3. In the top row of Figure 3 the fine structure and Fourier transform (FT) of Cl and S containing compounds are shown. The phase shift between **5** (GaS_6) and **4** (GaS_2N_4) is a result of the differing amounts of sulfur scatterers. The heavy scatterer S (Z = 16) and the light scatterer N (Z = 7) are out of phase.[37] **6** exhibiting a tetrahedral coordination geometry with four heavy chlorine scatterers (Z = 17) is phase shifted to both S and/or N containing fine structures. The difference in phase between **6** and **5** is mainly due to the differing Ga−Cl (2.16 Å) and Ga−S (2.43 Å) distances, and the first shell peak of **5** (GaS_6) in the FT is at higher R than for chlorine. Both spectra (**5** and **6**) show very uniform EXAFS oscillations over the whole k-range, indicating a uniformly distributed first shell made up of one type of atom.

1, **2**, and **3** are octahedral complexes with only O/N light scatterers in the first coordination shell exhibiting similar fine

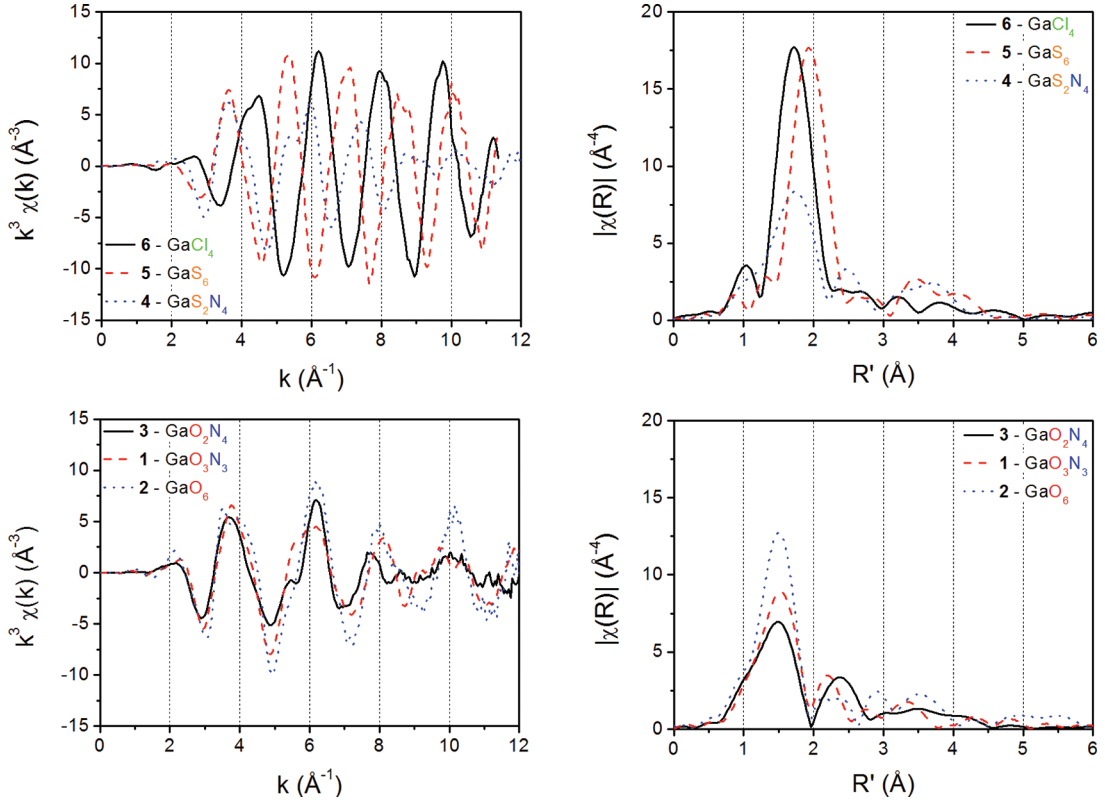

Figure 3. Extracted fine structures and Fourier transforms of the model compounds.

dx.doi.org/10.1021/jm3005459 | J. Med. Chem. 2012, 55, 5601−5613

Table 2. First Shell Fits of the Model Compounds Using Theoretical Amplitudes and Phases Provided by the FEFF Code[a]

compd	path	N_{fix}	R [Å]	R_{cryst} [Å]	ΔR [Å]	σ^2 [Å^2 10^{-3}]	E_0 [eV]	fit index [%]	cryst ref
6	Ga−Cl	4	2.167(3)	2.163	0.004	3.12 ± 1.22	3.0 ± 1.9	1.3	29
5	Ga−S	6	2.437(4)	2.433	0.004	2.35 ± 0.90	2.6 ± 1.4	2.3	28
4	Ga−S	2	2.40(6)	2.344	0.056	3.47 ± 1.22	2.5 ± 1.7	1.2	26
	Ga−N	4	2.09(6)	2.095	−0.005				
3	Ga−O	2	1.916(5)	1.912	0.004	2.49 ± 1.25	2.7 ± 1.6	1.3	25
	Ga−N	4	2.080(5)	2.075	0.005				
1	Ga−O	3	1.97(3)	1.944	0.026	2.41 ± 1.68	3.8 ± 2.7	2.1	2
	Ga−N	3	2.09(3)	2.077	0.013				
2	Ga−O	6	1.97(5)	1.946	0.024	4.53 ± 1.12	3.1 ± 1.7	0.9	24

[a] N_{fix} is the fixed coordination number. R is the average distance. R_{cryst} is the crystallographic value. ΔR is the difference between R and R_{cryst}. σ^2 is the Debye−Waller factor. E_0 is the residual shift of the edge energy.

Table 3. DL-EXCURV EXAFS Fits of the Model Compounds[a]

compd	path	N_{fix}	R [Å]	R_{cryst} [Å]	ΔR [Å]	σ^2 [Å^2 10^{-3}]	E_0 [eV]	R_{fit} [%]	fit index	cryst ref
6	Ga−Cl	4	2.159(3)	2.163	−0.004	3.38 ± 0.17	−6.8 ± 0.6	22.4	0.15	29
5	Ga−S	6	2.425(3)	2.433	−0.008	3.21 ± 0.19	−9.9 ± 0.5	24.4	0.15	28
4	Ga−N	4	2.08(1)	2.095	−0.015	5.85 ± 1.06	−8.4 ± 0.6	29.8	0.67	26
	Ga−S	2	2.376(7)	2.344	0.032	3.59 ± 0.71				
	Ga−C	4	3.03(2)	2.928	0.102	4.08 ± 2.06				
3	Ga−O	2	1.91(1)	1.912	−0.002	3.26 ± 1.26	−6.2 ± 0.7	26.4	0.50	25
	Ga−N	4	2.07(1)	2.075	−0.005	5.64 ± 1.42				
	Ga−N	2	2.52(3)	2.875	−0.355	9.95 ± 3.80				
	Ga−C	6	2.94(1)	2.943	−0.003	5.75 ± 1.32				
1	Ga−O	3	1.946(4)	1.944	0.002	1.84 ± 0.57	−7.2 ± 0.3	26.5	0.16	2
	Ga−N	3	2.077(6)	2.077	0.000	1.61 ± 0.71				
	Ga−C	6	2.811(5)	2.803	0.008	2.80 ± 0.42				
	Ga−C	9	3.94(1)	4.245	−0.305	7.27 ± 1.50				
2	Ga−O	6	1.957(5)	1.946	0.011	4.47 ± 0.47	−5.7 ± 0.6	29.5	0.57	24
	Ga−C	6	2.92(3)	2.891	0.029	9.93 ± 3.77				

[a] N_{fix} is the fixed coordination number. R is the average distance. R_{cryst} is the crystallographic value. ΔR is the difference between R and R_{cryst}. σ^2 is the Debye−Waller factor. E_0 is the residual shift of the edge energy. R_{fit} is the quality of the fit. Fit index is the sum of the square of the residuals.

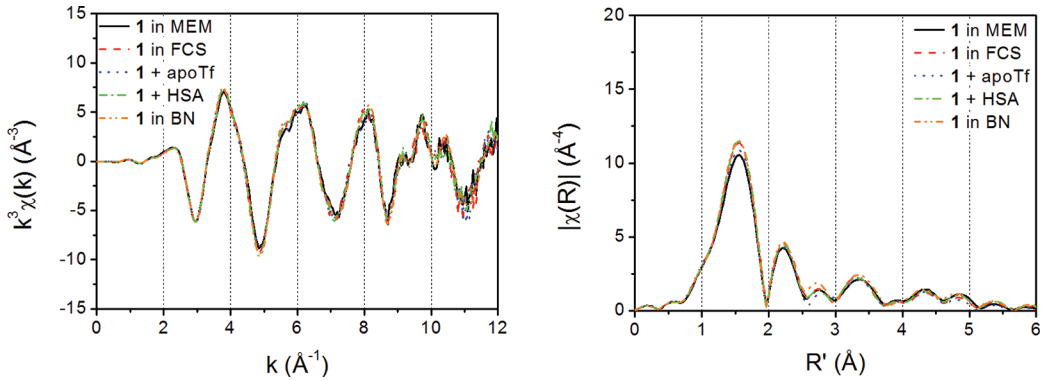

Figure 4. Extracted fine structures and Fourier transforms of **1** in the presence of minimum essential medium, fetal calf serum, apo-transferrin, and human serum albumin and as BN preparation.

structures. With increasing amount of oxygen ligands, the signal in the high k range becomes stronger, and the same is true for the amplitudes in the FT. This is in agreement with the reported oxygen and nitrogen distances for the different compounds.

The fitting analysis using FEFF[38,39] was restricted to the first coordination shell extracted from the first peak in the FT. The known information from the crystallographic data was taken as a starting point for the fits. The amount of scatterers was fixed not to exceed the number of fitting parameters. The results of the first shell fits of the model compounds using theoretical amplitudes and phases provided by the FEFF code are presented in Table 2.

The results for the DL-EXCURV[40] fits are given in Table 3. The distances are given as the average fitted distances for each atom type/shell (O/N, S, and C).

The curve fitting results obtained by FEFF and DL-EXCURV are both in good agreement with the crystallographic data. Thus, the reliability of the amplitude and phase shift extracted from **1** is confirmed.

KP46 in Presence of MEM, FCS, apoTf, and HSA. The k^3 weighted EXAFS spectra and the corresponding FT of **1** in the presence of MEM, FCS, apoTf, and HSA are shown in Figure 4. The extracted fine structures and FT for all five samples look

dx.doi.org/10.1021/jm3005459 | J. Med. Chem. 2012, 55, 5601−5613

Table 4. First Shell *q*-Space Fits of 1 in Presence of MEM, FCS, apoTf, and HSA with Amplitudes and Phases Provided by the FEFF Code[a]

compd	path	N_{fix}	R [Å]	σ^2 [Å^2 10^{-3}]	E_0 [eV]	fit index [%]
1	Ga−O	3	1.97(3)	2.41 ± 1.68	3.8 ± 2.7	2.1
	Ga−N	3	2.09(3)			
1 + FCS	Ga−O	3	1.98(3)	2.25 ± 1.81	3.6 ± 2.5	2.4
	Ga−N	3	2.10(4)			
1 + MEM	Ga−O	3	1.98(3)	2.62 ± 1.99	3.6 ± 2.7	2.8
	Ga−N	3	2.10(3)			
1 + HSA, 1:1	Ga−O	3	1.98(3)	2.13 ± 1.65	4.4 ± 2.3	2.1
	Ga−N	3	2.10(3)			
1 + apoTf, 1:1	Ga−O	3	1.98(3)	2.78 ± 1.96	3.2 ± 2.9	2.4
	Ga−N	3	2.09(3)			

[a] N_{fix} is the fixed coordination number. R is the average distance. σ^2 is the Debye−Waller factor. E_0 is the residual shift of the edge energy.

Table 5. DL-EXCURV EXAFS Fits of 1 in Presence of MEM, FCS, apoTf, and HSA[a]

compd	path	N_{fix}	R [Å]	σ^2 [Å^2 10^{-3}]	E_0 [eV]	R_{fit} [%]	fit index
1	Ga−O	3	1.946(4)	1.84 ± 0.57	−7.2 ± 0.3	26.5	0.16
	Ga−N	3	2.077(6)	1.61 ± 0.71			
	Ga−C	6	2.811(5)	2.80 ± 0.42			
	Ga−C	9	3.94(1)	7.27 ± 1.50			
1 + FCS	Ga−O	3	1.943(4)	1.38 ± 0.42	−7.3 ± 0.4	29.9	0.22
	Ga−N	3	2.083(7)	1.03 ± 0.23			
	Ga−C	9	2.830(7)	4.21 ± 0.72			
	Ga−C	3	3.94(2)	7.83 ± 2.11			
1 + MEM	Ga−O	3	1.938(6)	2.22 ± 0.73	−7.2 ± 0.4	30.2	0.23
	Ga−N	3	2.079(7)	1.59 ± 0.94			
	Ga−C	9	2.821(7)	4.85 ± 0.76			
	Ga−C	3	3.94(2)	8.08 ± 2.09			
1 + HSA, 1:1	Ga−O	3	1.943(5)	1.45 ± 0.65	−7.2 ± 0.4	28.0	0.19
	Ga−N	3	2.081(6)	1.02 ± 0.86			
	Ga−C	9	2.819(7)	4.28 ± 0.67			
	Ga−C	3	1.93(2)	8.78 ± 2.22			
1 + apoTf, 1:1	Ga−O	3	1.946(5)	2.41 ± 0.86	−7.2 ± 0.4	30.1	0.21
	Ga−N	3	2.076(9)	2.16 ± 1.14			
	Ga−C	9	2.834(7)	4.60 ± 0.74			
	Ga−C	3	3.92(2)	8.78 ± 2.26			

[a] N_{fix} is the fixed coordination number. R is the average distance. σ^2 is the Debye−Waller factor. E_0 is the residual shift of the edge energy. R_{fit} is the quality of the fit. Fit index is sum of the square of the residuals.

almost identical. The results of the XANES analysis are confirmed by the EXAFS data (Figure 4). The fits of the FEFF calculated theoretical spectra to the experimental ones are presented in Table 4. In Table 5 the results of the DL-EXCURV analysis are presented. The same structural model was used for fitting the experimental spectra of **1** in BN and in solution. The fits of the solution samples resemble the crystallographic data in the same way as shown in the fit for solid **1**.

KP46 in Mice Tumor and Liver Tissue. *XANES Analysis.* XANES spectra of tumor and liver samples from mice treated with **1** were collected at the synchrotrons in Hamburg (DESY) and Didcot (DLS). Because of the low concentration of gallium in these samples, no EXAFS signals could be collected. The XANES spectra from DLS were collected at spots high in Ga, identified with micro-XAS as described in the next paragraph. The tissue samples at DESY were collected with an unfocused beam. For the tumor and liver spectra measured at DLS, several spectra were collected at positions indicated by the crossing yellow lines in Figure 6 for the tumor and in Figure 7 for the liver sample.

The normalized XANES spectra and the corresponding first derivatives of the tumor and liver samples are coplotted with **1** in MEM in Figure 5. The edge positions of the XANES spectra taken from the tumor and liver material are all at 10 375.5 eV within 0.2 eV deviation. With respect to the low signal strength, the changes in the edge position are within statistical error and there is no evidence for a substantial change throughout the probed tissue samples. In comparison to the solid **1** in boron nitride and to **1** in MEM no significant shift in energy could be observed.

The white lines of the Ga XANES spectra from the tissue samples are slightly broadened, and the feature at about 10 385 eV, typical for **1**, is strongly attenuated. Similar features in other publications are assigned to multiple scattering effects.[32] The attenuation might be due to the higher degree of disorder in the complex tissue environment and the low signal-to-noise ratio.

The line shapes and spectral features are the same for tumor and liver samples treated with **1**. Different coordination of **1** in liver and tumor tissue is not assumed. From a XANES point of view, the three-dimensional coordination of the gallium from **1** in the tissue is nearly identical to **1** in boron nitride. Differences in

dx.doi.org/10.1021/jm3005459 | J. Med. Chem. 2012, 55, 5601−5613

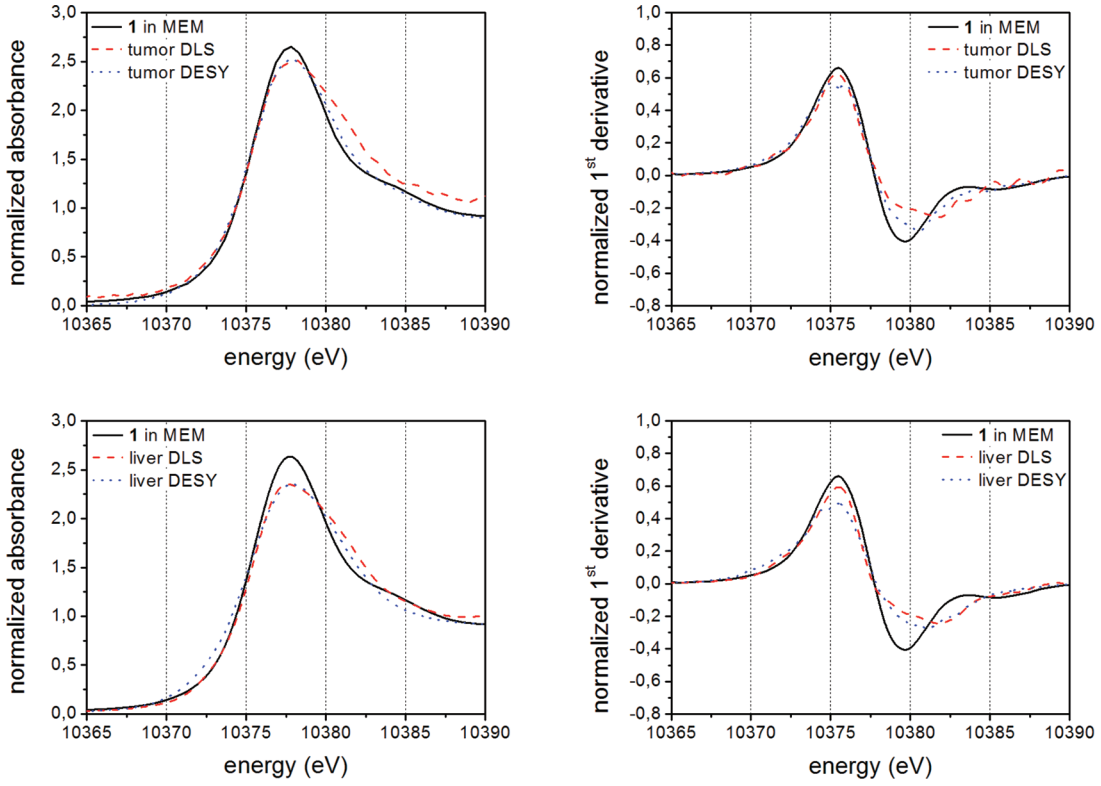

Figure 5. Tumor and liver XANES data and corresponding normalized first derivatives in comparison to **1** in MEM.

the white line heights are attributed to damping of the fluorescence signals because of the inhomogeneity of the tissue samples (thickness effects and pinholes).

Micro-XAS Analysis. Micro-XAS images of murine tumor and liver tissue were collected during two beam times in 2008 and 2011 to analyze the elemental distribution in the tissue samples, identifying regions of high gallium concentration. Simultaneous to the collection of gallium maps, the distribution patterns of Ca, Fe, Ni, Cu, and Zn were obtained, which made it possible to study the correlation of these elements with the Ga distribution pattern. In Figure 6 the micro-XAS maps of a murine tumor (sarcoma 180) are shown, and in Figure 7 the maps for a liver sample from the same individual are shown.

The maps show the distribution of Ga, Zn, Fe, Ca, Cu, and Ni. The tumor sample exhibits the same distribution pattern for Ga and Zn. The Fe distribution differs from that of Ga in the tumor tissue. The opposite is true for the liver sample where the Fe and Ga patterns are very similar but the Zn distribution is different. The distributions of Cu and Ni are similar in both samples, but the signals are much weaker. In contrast Ca shows a completely different distribution in both organs.

DISCUSSION

XAS methods were used to identify any changes in the coordination environment of **1** in the presence of two different serum proteins (HSA and apoTf) dissolved in culture medium (MEM) and fetal calf serum (FCS) and in vivo by analyzing liver and tumor samples originating from mice treated with **1**.

KP46 in Presence of MEM, FCS, apoTf, and HSA. MEM and FCS are widely used in cell culture. Therefore, the integrity and stability of **1** in these media are relevant for the conduction of reliable in vitro tests. The main constituents of MEM are inorganic salts, glucose, amino acids, and vitamins.[34] FCS comprises a variety of different amino acids and proteins[35] making up a large set of possible binding partners to the metal center. Since gallium reacts as a hard Lewis acid, oxygen and nitrogen should be preferential binding partners to Ga via the dissociation of one or more quinolinolato ligands or hydration through aqua ligands. Both events imply substantial changes in the coordination environment of gallium(III) and would have been clearly visible in the XANES and EXAFS spectra, as shown for the model compounds. The measured spectra are identical to each other and to the **1** boron nitride preparation.

The interaction of **1** with HSA and apoTf was previously investigated in other studies with capillary zone electrophoresis coupled with UV/vis detection (CZE−UV/vis)[33] and with capillary electrophoresis coupled to induced coupled plasma mass spectrometry (CE−ICP-MS) and electrospray ionization MS (CE−ESI-MS).[41] The hydrolytic stability and lipophilicity of the complex were tested with CZE−UV/vis and water/*n*-octanol partitioning tests,[33] respectively. The complex was stable under physiological conditions (at pH 7.4 in 10 mM NaH_2PO_4/Na_2HPO_4, 100 mM NaCl) with a half-life of $\tau_{1/2}$ = 14.2 h. The propensity to be more soluble in *n*-octanol than in water is caused by the rather lipophilic quinolinolato ligands. This opens the possibility of a non-transferrin mediated uptake of the drug into the cell through hydrophobic interactions. **1** was more reactive toward apoTf than toward HSA, showing very little reactivity toward the latter.[41] The overall affinity toward HSA and apoTf was very low in comparison to dissolved Ga salts.[41] The detection method used did not address the metal center directly but detected the formed adducts as a whole. Besides a covalent binding of the metal center to these molecules, a hydrophobic interaction is conceivable as well.

The XAS experiments in this study address the Ga center directly and provide valuable information about the possible binding situation. For the first time it is possible to address the

dx.doi.org/10.1021/jm3005459 | J. Med. Chem. 2012, 55, 5601−5613

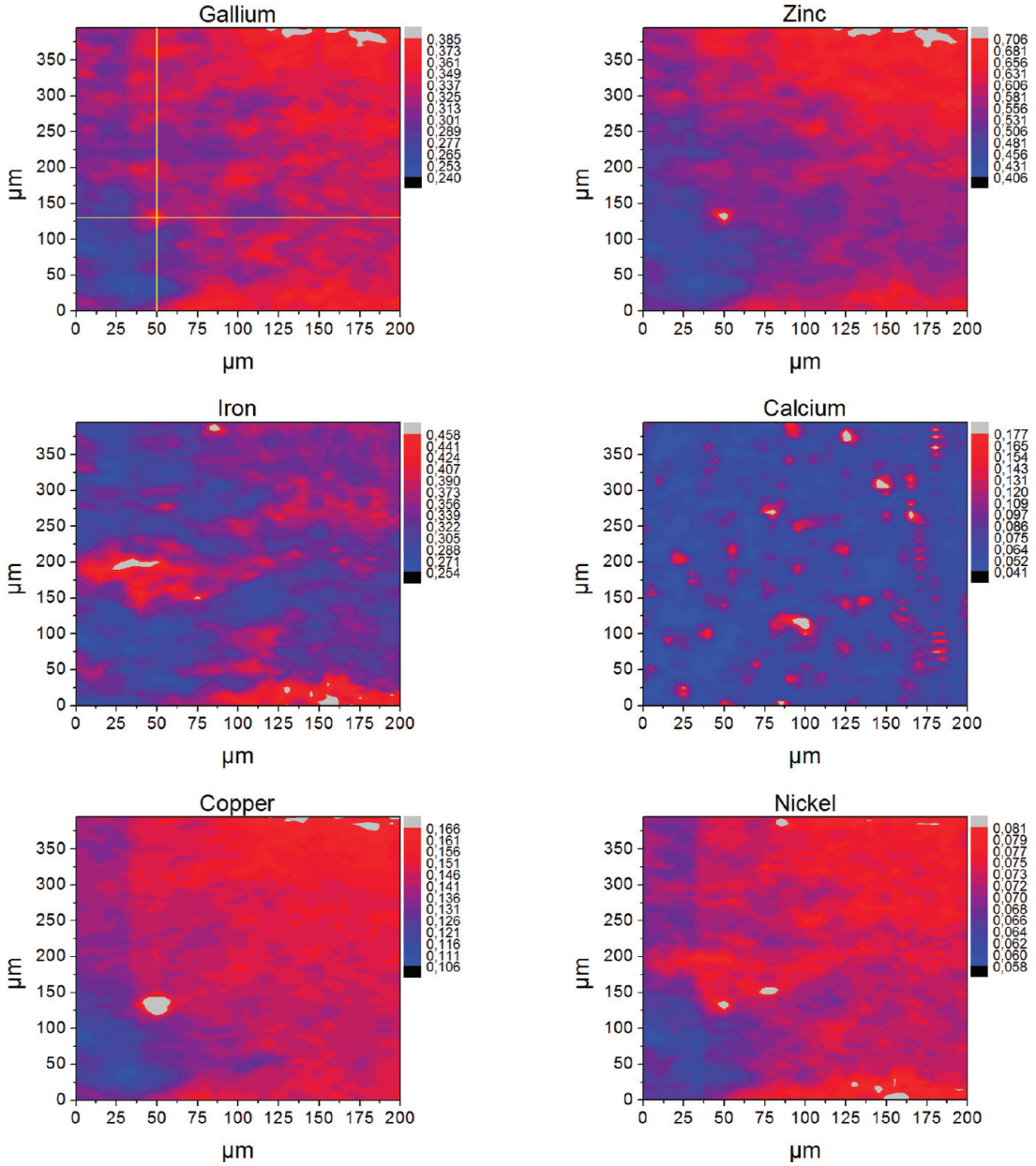

Figure 6. Normalized micro-XAS maps of tumor tissue. Upper limit of the color maps is the 99th percentile. Taken at beamline I18 at Diamond Light Source (U.K.).

atomic neighborhood of Ga in **1** in the presence of HSA and apoTf. When XAS was applied, no direct interaction or covalent bonding of the metal center toward HSA and apoTf could be found. This would have involved the dissociation of a ligand, easily detectable by XAS spectroscopy. Nonetheless an adduct formation between **1** and HSA or apoTf is not foreclosed by these results. More likely a noncovalent, more hydrophobic interaction could be the foundation of the underlying interaction mechanism. The stability of the complex under physiological conditions is emphasized by this XAS study. This counts for the majority of the molecules of **1**, since XAS measurements only describe the average coordination environment of all Ga atoms present in the sample.

KP46 in Tissue Samples. To date, no studies on the coordination of the metal center of **1** in biological tissue have been undertaken. In refs 42 and 43 a connection between the treatment of tumor cell lines with Ga nitrate and the internal Zn pool of these cells was drawn. In ref 42 gallium nitrate resistant and gallium nitrate sensitive cell lines were analyzed regarding their difference in the gene expression pattern of genes regulating the transition metal metabolism. It could be shown that gallium resistant cells showed a significantly higher expression of the metallothionein-2A gene (MT2A) and the zinc efflux transporter (ZnT-1). Both proteins are involved in the cellular handling of Zn. MT2A is an intracellular cystein-rich protein correlated to the handling of Zn, Cd, and certain other metals. ZnT-1 is a membrane based zinc efflux transporter. Gallium induces the expression of these proteins by the formation of reactive oxygen species (ROS). The increased oxidative stress initializes the metal-responsive transcription factor (MTF-1) related pathway, which in turn activates MT2A and ZnT-1 gene transcription.[43] These two proteins have a crucial impact on the intracellular Zn concentration, and Ga interfered with the expression patterns of these genes through the creation of ROS. Normally the

dx.doi.org/10.1021/jm3005459 | J. Med. Chem. 2012, 55, 5601−5613

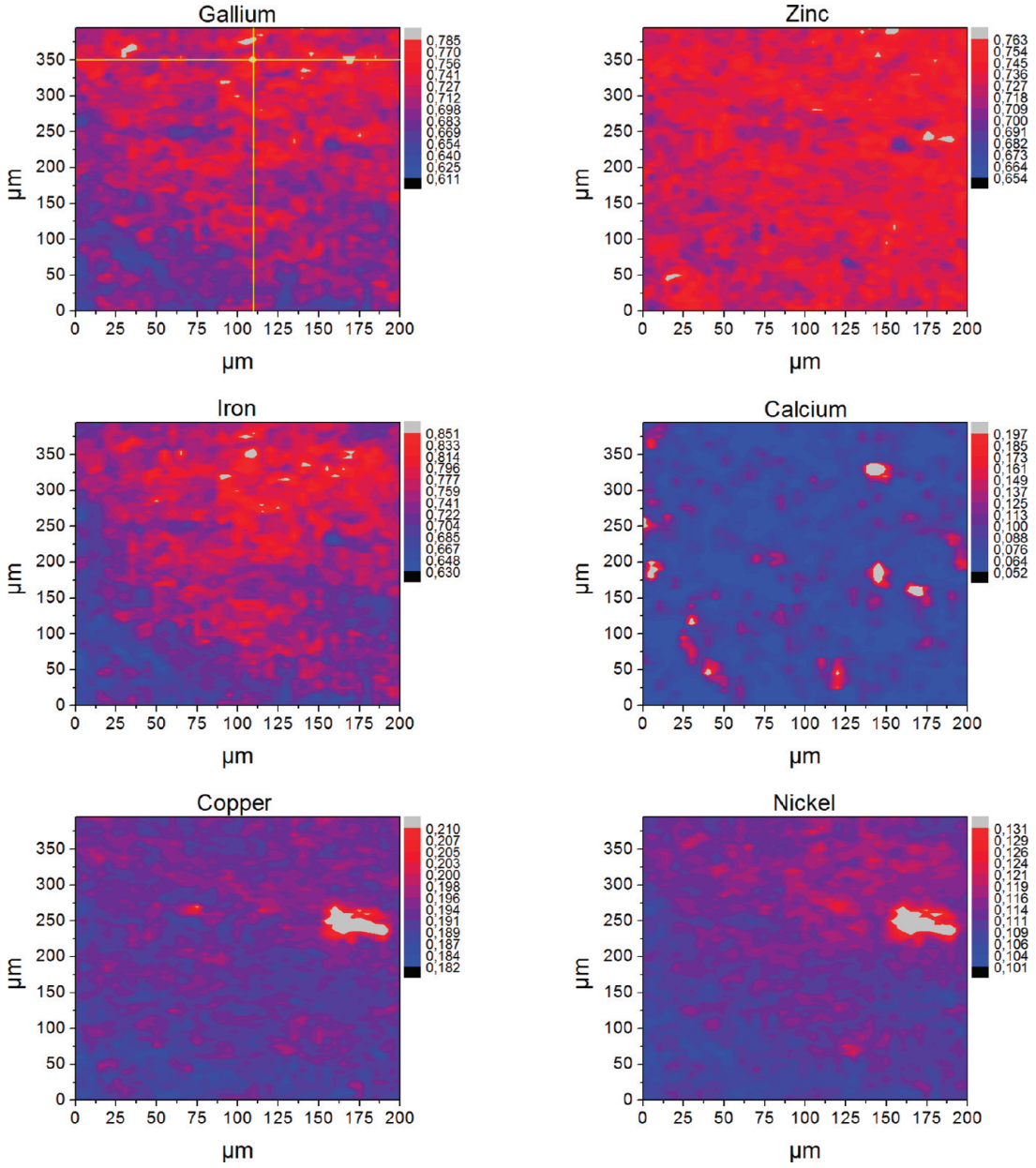

Figure 7. Normalized micro-XAS maps of liver tissue. Upper cutoff of the color maps is the 99th percentile. Taken at beamline I18 at Diamond Light Source (U.K.).

metallothionein-2A metabolism is strongly related to the divalent metals Zn and Cd. The metallothionein-2A expression is induced by Ga as well, a trivalent metal not occurring in the divalent state.

The results presented in this study demonstrate the correlation of Ga with the Zn distribution in tumor tissue. In the liver sample the Ga concentration was correlated to the Fe distribution pattern, which is not very surprising because these two ions are very similar. Similarities to other transition metals like Cu and Ni are given but to a minor degree. On the other side Ga patterns are absolutely independent from the Ca distribution (see Figure 6 and Figure 7). The XANES spectra collected at the low flux beamline D2 at DESY (unfocused beam) are the same as the spectra collected at the high flux beamline I18 at DLS ($5 \times 5\ \mu m^2$ focused beam) (Figure 5). A substitution of one ligand through a sulfur containing amino acid might have been a possible scenario in the biological samples and would have been clearly visible in the XANES spectra. In the collected XANES spectra (focused at DLS and unfocused at DESY) no substantial change in the immediate atomic environment of the metal center was observed.

CONCLUSIONS

XAS spectroscopy was applied to study **1** in vitro and in vivo. The basis of the analysis was provided by the examination of Ga model compounds with known coordination environments. The characterization of the model compounds was in good agreement with other studies undertaken on similarly coordinated Ga species in the past. No direct binding of the majority of the metal centers of **1** to the serum proteins HSA and apoTf could be detected. XAS further proved the stability of the complex under physiological conditions. The relative inertness of the metal center throughout the course from application to the target site in conjunction with the most likely drug carriers and reaction partners could be pointed out. With micro-XAS it was possible to

dx.doi.org/10.1021/jm3005459 | J. Med. Chem. 2012, 55, 5601−5613

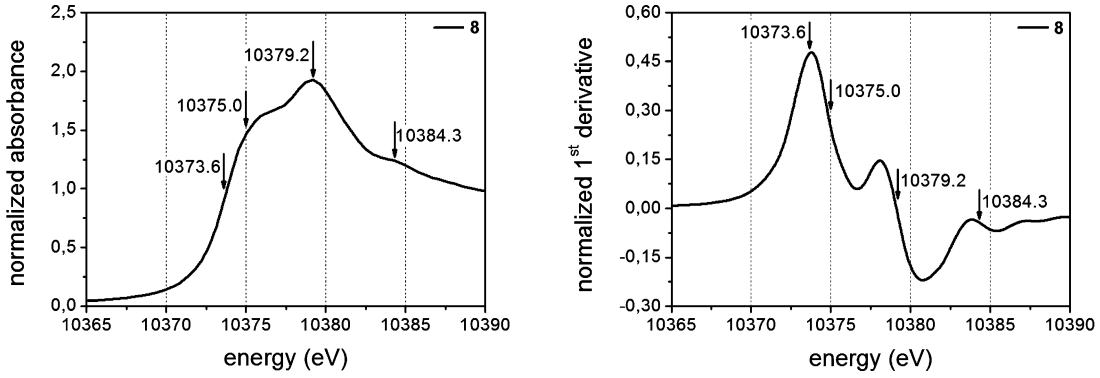

Figure 8. Normalized spectrum and first derivative of **8**.

investigate the distribution pattern of **1** in vivo and correlate it to the distribution patterns of other biological important metals like Ca, Fe, Cu, Ni, and Zn.

XANES spectra were collected at spots with a high content of Ga, revealing the local coordination of the metal center in vivo. The integrity of the majority of the molecules of **1** in mouse tumor and liver tissue was confirmed.

XAS has proven to be a very powerful tool for the investigation of metallodrugs in a variety of test systems missing any long-range order. The sensitivity of the method to small changes in the ligand environment and the ability to detect the elements of question in trace amounts were proved.

EXPERIMENTAL SECTION

Sample Preparation. The model compounds were diluted in boron nitride (Sigma Aldrich, CAS no. 10043-11-5, 99.5% BN) to a calculated absorption of about 1 AU following standard procedures.[44] Aluminum sample holders were filled with the samples and sealed with Kapton foil.

The solution samples were prepared according to previously described procedures.[41] Human serum albumin (HSA) from plasma, human apo-transferrin (apoTf), minimum essential medium (MEM), fetal calf serum (FCS), sodium bicarbonate, disodium hydrogenphosphate, sodium chloride, glycerol, and dimethylsulfoxide (DMSO) where purchased from Sigma Aldrich. Phosphate buffered saline (PBS) (pH 7.4) was prepared according to standard procedures.[41] Stock solutions of 10 mM **1** in DMSO, 1.5 mM apoTf in PBS, and 1.5 mM HSA in PBS were prepared. The final solutions of **1** were prepared by mixing 10% (v/v) **1** in DMSO, 70% (v/v) of the biomolecule stock solutions, and 20% (v/v) of glycerol. Before the glycerol was added, the solutions were incubated at 37 °C for 30 min. After the incubation, the aluminum sample holders were filled with the solutions and sealed with Kapton foil. The samples were flash frozen in liquid nitrogen and stored at −85 °C. The following solutions were prepared: 1 mM **1** in MEM, 1 mM **1** in FCS, 1:1 mM **1** + apoTf in DMSO/PBS, 1:1 mM **1** + HSA in DMSO/PBS.

The tissue samples were taken from experiments performed in accordance with the European Community Guidelines for the use of experimental animals in the animal facility at the Cancer Research Institute, Slovak Academy of Sciences, Bratislava, Slovak Republic. BALB/c mice bearing the subcutaneous sarcoma 180 were treated with **1** in the following way: **1** was suspended in a Tween-60/H_2O, 1:4, solution and applied orally in a dosage of 200 mg kg^{-1} day^{-1} on 6 consecutive days. Tumor and liver were collected 1 day after the last drug administration and stored at −80 °C. Samples of these were placed into aluminum sample holders. The holders were sealed with Kapton foil, and the samples were flash frozen in liquid nitrogen. The following tissue samples were measured: tumor at DLS, tumor at DESY, liver at DLS, liver at DESY.

XAS Experiments. The XANES and EXAFS experiments were carried out at two different synchrotron radiation facilities and beamlines: beamline D2 at the Deutsche Elektronen Synchrotron (DESY) in Hamburg (Germany) and beamline I18 at the Diamond Light Source (DLS) in Didcot (England). The micro-XAS maps of the tissue samples were collected at DLS.

The model compounds were measured in transmission mode. All other spectra and the micro-XAS maps were collected in fluorescence mode. Dead time correction was applied to the fluorescence spectra. The beamline D2 at DESY was equipped with a Si(111) double crystal monochromator and a Canberra 13 element solid state Ge detector for fluorescence measurements. The DORIS synchrotron was operated at 4.5 GeV. The beamline I18 at DLS was equipped with a double crystal Si(111) monochromator and 27 mm period undulator giving an energy range of 2−20.7 keV (flux of 4×10^{12} ph/s). Higher harmonics were rejected using two plane mirrors with Rh and Ni stripes. For the micro-XAS maps and XANES of the tissue samples the beam was focused with mechanical Kirkpatrick−Baez mirrors with Si and Rh stripes to a spot size of 5×5 μm^2. The signal was detected with ionization chambers in transmission and a nine element solid state Ge detector in fluorescence mode. The Diamond synchrotron was operated at 3 GeV with an electron beam current of 250−150 mA. All tissue and solution samples were measured at cryogenic temperatures (about 50 K) using an Oxford Instruments MicroRes He cryostat. The model BN preparations were measured at room temperature, whereas at DESY all measurements were conducted at cryogenic temperatures of around 20 K.

The XANES signals were measured at the Ga K-edge with a pre-edge region from 10 217 to 10 340 eV with a step size of 6 eV, an edge region from 10 340 to 10 402 eV with a step size of 0.5 eV. The scanning times were set to 1 s in the pre-edge and 2 s in the edge region. The *k*-space was measured from 3 to 8 $Å^{-1}$ with a step size of 0.05 $Å^{-1}$. The postedge scanning time was increased according to a predefined exponential-like curve from 1 to 6 s.

The EXAFS modulations were measured at the Ga K-edge with pre-edge and edge settings as used in the XANES measurements. The *k*-space was measured from 3 to 14 $Å^{-1}$ with a step size of 0.04 $Å^{-1}$. The scanning times were 1 s in the pre-edge (10217−10240 eV), 2 s in the edge (10340−10402 eV), and 2−8 s (10402−11110 eV), increasing according to a predefined curve, in the postedge region.

The micro-XAS maps were collected at beamline I18 at DLS with a fixed energy of 12 keV. The beam was focused to a spot size of 5×5 μm^2, and the fluorescence signals were collected for 3 s at each spot. The XANES spectra of the tissue samples from DLS were measured with a focused beam as well. The spots high in gallium where the XANES spectra were taken are marked in Figure 6 and Figure 7 (crossing yellow lines).

Energy Calibration. The monochromator stability was proven, and the energy calibration was performed by measuring gallium oxide (**8**, β-Ga_2O_3) every two sample scans. **8** was purchased from Sigma Aldrich (Puratronic 99.999%, CAS no. 12024-21-4) and measured as BN preparation.

In accordance with previous studies[32,45] on **8** three significant features in the XANES spectra could be determined: an edge shoulder at 10 375.0 eV, a postedge peak at 10 379.2 eV, and a third small peak at about 10 385 eV (Figure 8). The edge position lies at 10 373.5 eV and was determined as the inflection point on the rising edge of the XANES

dx.doi.org/10.1021/jm3005459 | J. Med. Chem. 2012, 55, 5601−5613

spectrum. The spectrum of **8** constitutes an overlay of tetrahedral (Ga(t)) and octahedral (Ga(o)) gallium.[32] The absorption maximum of Ga(t) lies at 10 375.0 eV, represented as an edge shoulder in Figure 8. The one of Ga(o) lies at 10 379.2 eV, also seen as a postedge peak in Figure 8.

The energy calibration was done using the postedge peak at 10 379.2 eV by applying the software packages ATHENA[46] and IFEFFIT.[47] In Figure 8 the normalized spectrum and the first derivative of **8** are shown.

XAS Analysis. The program packages ATHENA, ARTEMIS,[46] FEFF,[38,39] EXPROG,[48] PySpline,[49] and DL-EXCURV[40] were applied for XAS data analysis.

XANES Analysis. The pre-edge background was removed by a linear approximation in the range of −50 to −150 eV before the edge. This baseline was subtracted from the entire spectrum. The normalization was accomplished by fitting a quadratic polynomial in the postedge region from 150 to 240 eV. The function was extrapolated to the first absorption maximum, and the absorbance was set to unity there. The edge position was determined as the maximum in the first derivative of the spectrum (inflection point of the steeply rising edge). The spectra were shifted according to the observed shift for the standard compound **8** (E_0 = 10 373.6 eV; see Figure 8).

EXAFS Analysis. *FEFF Analysis.* The pre-edge background subtraction and the normalization were performed as described for the XANES spectra. The normalized EXAFS signals were extracted using the AUTOBK algorithm incorporated into IFEFFIT.[47] The background function is constructed using cubic splines with evenly spaced knots throughout the data region. The number of splines is defined as $(2R_{bkg}\Delta k)/\pi$, where R_{bkg} defines the frequencies that are allowed to be removed by the smoothly varying background spline and is usually set to one-half of the first shell distance (longer frequencies will be removed). In our case R_{bkg} was set to 1 Å and the spline range Δk to 0.5−13.5 Å^{-1}. The Fourier transform was constructed using a Hanning window from 2 to 10 Å^{-1} and a δk of 2 Å^{-1}. The back-Fourier transform was extracted using a Hanning window from 1 to 2 Å and a δR of 0 Å.

FEFF 7[50] was used for the calculation of the theoretical EXAFS amplitudes and phases. The input file for the FEFF code was created out of the structural model of **1**[1] described below and the crystallographic first shell data of the model compounds, respectively. The program package ARTEMIS[46] was used to make the least-squares fits of the theoretical spectra to the experimental ones. The shift in the edge position (E_0) and the mean square relative displacement (σ^2, Debye−Waller factor) were refined for all scattering paths. The absorber−scatterer distance (R) was defined over a contraction expansion factor α relative to the starting values of the structural models. The amplitude reduction factor S_0^2 was set to a fixed value of 1.0, which allows the correct comparison of the different fits. The coordination number N was set according to the crystallographic value to not exceed the number of free parameters. The first shell fits were performed on the back-transformed, Fourier filtered spectra.

DL-EXCURV Analysis. The k^3 weighted EXAFS signals were obtained using the program PySpline. The edge energy was set to the values as determined in the XANES analysis. The pre-edge background was fitted through a straight line and subtracted from the entire spectrum. The postedge background was fitted using a three-segment spline buildup of third order polynomials. The FT was constructed using a Kaiser−Bessel window with δk = 0.1 Å^{-1}. DL-EXCURV calculated the theoretical EXAFS spectra for the defined structural model based on the curved wave method for single scattering. The ground- and excited-state exchange contributions to the effective potential were calculated with the von Barth method.[51] The structural parameters atomic distance (R), Debye−Waller factor ($2\sigma^2$), and the residual shift (EF) of the edge energy (E_0) were refined to obtain the best fit between experiment and theory. The amplitude reduction factor (AFAC) and the number of scatterers (N) were fixed. The quality of the fit was indicated by the R-factor.[52] The number of free parameters (N_P) was always inspected to be less than the number of independent data points (N_{IND}).[53] The fits were performed on the raw k^3 weighted EXAFS data.

Structural Model. The minimal distinguishable distances are determined according to the formula $\delta R = \pi/(2k_{max})$,[54,55] where k_{max} represents the upper limit used for the Fourier transformation. For **1** δR = 0.157 Å and is in the same range as the most distant O and N atoms in our crystallographic model (δR_{eff} = 0.162 Å). This makes it possible to distinguish these two first shell atom species and perform subshell fits for O and N and determine their mean distance to the central Ga atom. The first shell was built up of the three O atoms at distances from 1.937 to 1.950 Å and three N atoms with distances from 2.061 to 2.099 Å. The calculated mean distances Ga−O and Ga−N for **1** were 1.944 and 2.077 Å, respectively.

Micro-XAS Analysis. The micro-XAS maps were analyzed using the program package PyMCA.[56] The maps were constructed by normalizing the fluorescence signals with the incoming X-ray beam intensity I_0. The upper limit for the signals was set to the 99th percentile to remove unwanted signal peaks due to detector glitches.

AUTHOR INFORMATION

Corresponding Author

*Phone: +43-1-427752501. Fax: +43-1-42779525. E-mail: annette.rompel@univie.ac.at.

Notes

The authors declare no competing financial interest.

ACKNOWLEDGMENTS

Financial support by the Deutsche Forschungsgemeinschaft, DFG (Grant RO1084/7-1), is gratefully acknowledged. This work was carried out with the support of the Diamond Light Source. Portions of this research were carried out at the light source DORIS D2 beamline (EMBL outstation) at DESY, a member of the Helmholtz Association (HGF). The work was also supported by means of the European Commission FP7 Program ELISA. A Ga fluorescence map was taken on a mouse liver sample treated with **1** at the Swiss Light Source with a spot size of 2 × 2 μm^2 for initial experiments. EXAFS data were taken at a high concentration spot on the map (data not shown). The EXAFS on the hot spot showed the characteristic spectrum of **1**. We highly acknowledge the support of Dr. D. Grolimund and Dr. C. Borca of Swiss Light Source, Paul Scherrer Institute, Villigen, Switzerland. Prof. L. Novotny and Dr. P. Rauko (Cancer Research Institute, Slovak Academy of Sciences, Bratislava, Slovak Republic) are acknowledged for providing tumors and organs from in vivo experiments.

ABBREVIATIONS USED

XAS, X-ray absorption spectroscopy; XANES, X-ray absorption near edge structure; EXAFS, extended X-ray absorption fine structure; micro-XAS, micro X-ray absorption spectroscopy; BN, boron nitride; MEM, minimum essential medium; HSA, human serum albumin; DMSO, dimethylsulfoxide; DESY, Deutsches Elektronen Synchrotron; DLS, Diamond Light Source Ltd.; FT, Fourier transform; ph, photon; AU, absorbance unit

REFERENCES

(1) Collery, P.; Domingo, J. L.; Keppler, B. K. Preclinical toxicology and tissue gallium distribution of a novel antitumour gallium compound: tris(8-quinolinolato)gallium(III). *Anticancer Res.* **1996**, *16*, 687−691.

(2) Wang, Y.; Zhang, W.; Li, Y.; Ye, L.; Yang, G. X-ray crystal structure of gallium tris(8-hydroxyquinoline): intermolecular pi−pi stacking interactions in the solid state. *Chem. Mater.* **1999**, *11*, 530−532.

(3) Hofheinz, R. D.; Dittrich, C.; Jakupec, M. A.; Drescher, A.; Jaehde, U.; Gneist, M.; Graf von Keyserlingk, N.; Keppler, B. K.; Hochhaus, A. Early results from a phase I study on orally administered tris(8-quinolinolato)gallium(III) (FFC11, KP46) in patients with solid tumors: a CESAR study (Central European Society for Anticancer Drug Research—EWIV). *Int. J. Clin. Pharmacol. Ther.* **2005**, *43*, 590−591.

(4) Collery, P.; Lechenault, F.; Cazabat, A.; Juvin, E.; Khassanova, L.; Evangelou, A.; Keppler, B. Inhibitory effects of gallium chloride and tris(8-quinolinolato)gallium(III) on A549 human malignant cell line. *Anticancer Res.* **2000**, *20*, 955−958.
(5) Hart, M. M.; Adamson, R. H. Antitumor activity and toxicity of salts of inorganic group IIIa metals: aluminum, gallium, indium, and thallium. *Proc. Natl. Acad. Sci. U.S.A.* **1971**, *68*, 1623−1626.
(6) Hart, M. M.; Smith, C. F.; Yancey, S. T.; Adamson, R. H. Toxicity and antitumor activity of gallium nitrate and periodically related metal salts. *J. Natl. Cancer Inst.* **1971**, *47*, 1121−1127.
(7) Straw, J. A.; Klubes, P.; Hart, M. M. Distribution of anticancer agents in spontaneous animal tumors. II. Distribution of gallium in canine lymphosarcoma. *J. Natl. Cancer Inst.* **1975**, *55*, 199−202.
(8) Jakupec, M.; Keppler, B. K. Gallium in cancer treatment. *Curr. Top. Med. Chem.* **2004**, *4*, 1575−1583.
(9) Bernstein, L. R.; Tanner, T.; Godfrey, C.; Noll, B. Chemistry and pharmacokinetics of gallium maltolate, a compound with high oral gallium bioavailability. *Met.-Based Drugs* **2000**, *7*, 33−47.
(10) Collery, P.; Millart, H.; Pechery, C.; Kratz, F.; Keppler, B. K. New Gallium Complexes for a Cisplatin Combination Therapy. In *Metal Ions in Biology and Medicine*; John Libbey Eurotext: Paris, 1992; Vol. *2*, pp 173−175.
(11) Collery, P.; Keppler, B.; Madoulet, C.; Desoize, B. Gallium in cancer treatment. *Crit. Rev. Oncol./Hematol.* **2001**, *42*, 283−296.
(12) Desoize, B.; Jardillier, J.-C. Multicellular resistance: a paradigm for clinical resistance? *Crit. Rev. Oncol./Hematol.* **2000**, *36*, 193−207.
(13) Collery, P.; Jakupec, M. A.; Kynast, B.; Keppler, B. K. Preclinical and Early Clinical Development of the Antitumor Gallium Complex KP46 (FFC11). In *Metal Ions in Biology and Medicine*; John Libbey Eurotext: Paris, 2006; Vol. *9*, pp 521−524.
(14) Valiahdi, S. M.; Heffeter, P.; Jakupec, M. A.; Marculescu, R.; Berger, W.; Rappersberger, K.; Keppler, B. K. The gallium complex KP46 exerts strong activity against primary explanted melanoma cells and induces apoptosis in melanoma cell lines. *Melanoma Res.* **2009**, *19*, 283−293.
(15) Bernstein, L. R. Mechanisms of therapeutic activity for gallium. *Pharmacol. Rev.* **1998**, *50*, 665−682.
(16) Chitambar, C.; Matthaeus, W.; Antholine, W.; Graff, K.; O'Brien, W. Inhibition of leukemic HL60 cell growth by transferrin-gallium: effects on ribonucleotide reductase and demonstration of drug synergy with hydroxyurea. *Blood* **1988**, *72*, 1930−1936.
(17) Chitambar, C. R.; Narasimhan, J. Targeting iron-dependent DNA synthesis with gallium and transferrin-gallium. *Pathobiology* **1991**, *59*, 3−10.
(18) Chitambar, C. R.; Zivkovic-Gilgenbach, Z.; Narasimhan, J.; Antholine, W. E. Development of drug resistance to gallium nitrate through modulation of cellular iron uptake. *Cancer Res.* **1990**, *50*, 4468−4472.
(19) Yano, J.; Yachandra, V. K. X-ray absorption spectroscopy. *Photosynth. Res.* **2009**, *102*, 241−254.
(20) Penner-Hahn, J. E. Characterization of "spectroscopically quiet" metals in biology. *Coord. Chem. Rev.* **2005**, *249*, 161−177.
(21) Ascone, I.; Meyer-Klaucke, W.; Murphy, L. Experimental aspects of biological X-ray absorption spectroscopy. *J. Synchrotron Radiat.* **2002**, *10*, 16−22.
(22) Ascone, I.; Strange, R. Biological X-ray absorption spectroscopy and metalloproteomics. *J. Synchrotron Radiat.* **2009**, *16*, 413−421.
(23) Yano, J.; Kern, J.; Irrgang, K.-D.; Latimer, M. J.; Bergmann, U.; Glatzel, P.; Pushkar, Y.; Biesiadka, J.; Lolll, B.; Sauer, K.; Messinger, J.; Zouni, A.; Yachandra, V. K. X-ray damage to the Mn_4Ca complex in single crystals of photosystem II: a case study for metalloprotein crystallography. *Proc. Natl. Acad. Sci. U.S.A.* **2005**, *102*−*34*, 12047−12052.
(24) Bhattacharya, S.; Singh, S.; Gupta, V. D. A structural study on gallium and indium beta-diketonates. *J. Chem. Crystallogr* **2002**, *32*, 299−305.
(25) Dobrov, A.; Arion, V. B.; Kandler, N.; Ginzinger, W.; Jakupec, M. A.; Rufińska, A.; Graf von Keyserlingk, N.; Galanski, M.; Kowol, C.; Keppler, B. K. The first metal-based paullone derivative with high antiproliferative activity in vitro. *Inorg. Chem.* **2006**, *45*, 1945−1950.
(26) Kowol, C. R.; Berger, R.; Eichinger, R.; Roller, A.; Jakupec, M. A.; Schmidt, P. P.; Arion, V. B.; Keppler, B. K. Gallium(III) and iron(III) complexes of α-N-heterocyclic thiosemicarbazones: synthesis, characterization, cytotoxicity, and interaction with ribonucleotide reductase. *J. Med. Chem.* **2007**, *50*, 1254−1265.
(27) Andrews, P. C.; Lawrence, S. M.; Raston, C. L.; Skelton, B. W.; Tolhurst, V.-A.; White, A. H. Dithiocarbamate complexes of trivalent aluminium and gallium via metal hydrides. *Inorg. Chim. Acta* **2000**, *300*−*302*, 56−64.
(28) Dymock, K.; Palenik, G. J.; Slezak, J.; Raston, C. L.; White, A. H. Crystal structures of tris(diethyldithiorcarbamato)-gallium(III) and indium(III). *J. Chem. Soc., Dalton Trans.* **1976**, 28−32.
(29) Jakubas, R.; Bator, G.; Góniowska, M.; Ciunik, Z.; Baran, J.; Lefebvre, J. Crystal structure and phase transition of $[(CH_3)_2NH_2]$-$GaCl_4$. *J. Phys. Chem. Solids* **1997**, *58*, 989−998.
(30) Chitamber, C. R. Gallium compounds as antineoplastic agents. *Curr. Opin. Oncol.* **2004**, *16*, 547−552.
(31) Hendsbee, A. D.; Pye, C. C.; Masuda, J. D. Hexaaquagallium(III) trinitrate trihydrate. *Acta Crystallogr., Sect. E: Struct. Rep. Online* **2009**, *65*, i65.
(32) Nishi, K.; Shimizu, K.; Takamatsu, M.; Yoshida, H.; Satsuma, A.; Tanaka, T.; Yoshida, S.; Hattori, T. Deconvolution analysis of Ga K-Edge XANES for quantification of gallium coordinations in oxide environments. *J. Phys. Chem. B* **1998**, *102*, 10190−10195.
(33) Rudnev, A. V.; Foteeva, L. S.; Kowol, C.; Berger, R.; Jakupec, M. A.; Arion, V. B.; Timerbaev, A. R.; Keppler, B. K. Preclinical characterization of anticancer gallium(III) complexes: solubility, stability, lipophilicity and binding to serum proteins. *J. Inorg. Biochem.* **2006**, *100*, 1819−1826.
(34) *Bacteriological Analytical Manual/Food and Drug Administration*, 8th ed., revision A; AOAC International: Gaithersburg, MD, 1998.
(35) Honn, K. V.; Singley, J. A.; Chavin, W. Fetal bovine serum: a multivariate standard. *Proc. Soc. Exp. Biol. Med.* **1975**, *149*, 344−347.
(36) Harris, W. R.; Messori, L. A comparative study of aluminum(III), gallium(III), indium(III), and thallium(III) binding to human serum transferrin. *Coord. Chem. Rev.* **2002**, *228*, 237−262.
(37) Clark-Baldwin, K.; Tierney, D. L.; Govindaswamy, N.; Gruff, E. S.; Kim, C.; Berg, J.; Koch, S. A.; Penner-Hahn, J. E. The limitations of X-ray absorption spectroscopy for determining the structure of zinc sites in proteins. When is a tetrathiolate not a tetrathiolate? *J. Am. Chem. Soc.* **1998**, *120*, 8401−8409.
(38) Ankudinov, A. L.; Ravel, B.; Rehr, J. J.; Conradson, S. D. Real-space multiple-scattering calculation and interpretation of X-ray-absorption near-edge structure. *Phys. Rev. B* **1998**, *58*, 7565−7576.
(39) Rehr, J. J.; Albers, R. C. Theoretical approaches to X-ray absorption fine structure. *Rev. Mod. Phys.* **2000**, *72*, 621−654.
(40) Tomic, S.; Searle, B. G.; Wander, A.; Harrison, M. N.; Dent, A. J.; Mosselmans, J. F. W.; Ingelsfield, J. E. *New Tools for the Analysis of EXAFS: The DL EXCURV Package*; CCLRC Technical Report; Council for the Central Laboratory of the Research Councils: U.K., 2005.
(41) Groessl, M.; Bytzek, A.; Hartinger, C. G. The serum protein binding of pharmacologically active gallium (III) compounds assessed by hyphenated CE-MS techniques. *Electrophoresis* **2009**, *30*, 2720−2727.
(42) Yang, M.; Kroft, S. H.; Chitambar, C. R. Gene expression analysis of gallium-resistant and gallium-sensitive lymphoma cells reveals a role for metal-responsive transcription factor-1, metallothionein-2A, and zinc transporter-1 in modulating the antineoplastic activity of gallium nitrate. *Mol. Cancer Ther.* **2007**, *6*, 633−643.
(43) Yang, M.; Chitambar, C. R. Role of oxidative stress in the induction of metallothionein-2A and heme oxygenase-1 gene expression by the antineoplastic agent gallium nitrate in human lymphoma cells. *Free Radical Biol. Med.* **2008**, *45*, 763−772.
(44) Kelly, S. D.; Hesterberg, D.; Ravel, B. Analysis of Soils and Minerals Using X-ray Absorption Spectroscopy. In *Methods of Soil Analysis. Part S. Mineralogical Methods*; Ulery, A. L., Drees, L. R., Eds.; Soil Science Society of America: Madison, WI, 2008; pp 387−463.

(45) Wei, A. C.; Liu, P. H.; Chao, K. J.; Yang, E.; Cheng, H. Y. X-ray absorption measurement and density functional theory analysis of gallium in gallium-containing beta zeolites. *Microporous Mesoporous Mater.* **2001**, *47*, 147−156.
(46) Ravel, B.; Newville, M. ATHENA, ARTEMIS, HEPHAESTUS: data analysis for X-ray absorption spectroscopy using IFEFFIT. *J. Synchrotron Radiat.* **2005**, *12*, 537−541.
(47) Newville, M. IFEFFIT: interactive XAFS analysis and FEFF fitting. *J. Synchrotron Radiat.* **2001**, *8*, 322−324.
(48) Nolting. H.-F.; Hermes, C. *EXPROG: EMBL EXAFS Data Analysis and Evaluation Program Package for PC/AT*; European Molecuar Biology Laboratory, c/o DESY: Hamburg, Germany, 1992.
(49) Tenderholt, A.; Hedman, B.; Hodgson, K. O. Pyspline: a modern, cross-platform program for the processing of raw averaged XAS edge and EXAFS data. *AIP Conf. Proc.* **2007**, *882*, 105−107.
(50) Ankudinov, A. L.; Rehr, J. J. Relativistic calculations of spin-dependent X-ray-absorption spectra. *Phys. Rev. B* **1997**, *56*, 1712−1716.
(51) von Barth, U.; Hedin, L. A local exchange-correlation potential for the spin polarized case. *J. Phys. C: Solid State Phys.* **1972**, *5*, 1629−1642.
(52) Binsted, N.; Strange, R. W.; Hasnain, S. S. Constrained and restrained refinement in EXAFS data analysis with curved wave theory. *Biochemistry* **1992**, *31*, 12117−12125.
(53) Stern, E. A. Number of relevant independent points in X-ray-absorption fine-structure spectra. *Phys. Rev. B* **1993**, *48*, 9825−9827.
(54) Messori, L.; Balerna, A.; Ascone, I.; Castellano, C.; Gabbiani, C.; Casini, A.; Marchioni, C.; Jaouen, G.; Congiu Castellano, A. X-ray absorption spectroscopy studies of the adducts formed between cytotoxic gold compounds and two major serum proteins. *J. Biol. Inorg. Chem.* **2010**, *16*, 491−499.
(55) Bunker, G. *Introduction to XAFS: A Practical Guide to X-ray Absorption Fine Structure Spectroscopy*, 1st ed.; Cambridge University Press: Cambridge, U.K., 2010.
(56) Solé, V. A.; Papillon, E.; Cotte, M.; Walter, P.; Susini, J. A multiplatform code for the analysis of energy-dispersive X-ray fluorescence spectra. *Spectrochim. Acta, Part B* **2007**, *62*, 63−68.